

## Article

# High-Temperature Cracking of Pentene to Ethylene and Propylene over H-ZSM-5 Zeolites: Effect of Reaction Conditions and Mechanistic Insights

Yueyang Han, Lingyin Du, Yuan Zhu, Youhao Xu \*, Xuhui Bai, Ying Ouyang, Yibin Luo and Xingtian Shu

Research Institute of Petroleum Processing, Sinopec, Beijing 100083, China

\* Correspondence: xuyouhao.ripp@sinopec.com; Tel.: +86-010-8236-8427

**Abstract:** The effects of reaction conditions on the yield of ethylene and propylene from pentene cracking were investigated in a fixed-bed reactor at 500–750 °C and for a weight hourly space velocity (WHSV) of 15–83 h<sup>-1</sup>. The total yield of ethylene and propylene reached a maximum (67.8 wt%) at 700 °C and 57 h<sup>-1</sup>. In order to explore the reaction mechanism at high temperatures, a thermal/catalytic cracking proportion model was established. It was found that the proportion of pentene feed chemically adsorbed with the acid sites and cracked through catalytic cracking was above 88.4%, even at 750 °C. Ethylene and propylene in the products were mainly derived from catalytic cracking rather than thermal cracking at 650–750 °C. In addition, the suitable reaction network for pentene catalytic cracking was deduced and estimated. The results showed that the monomolecular cracking proportion increased from 1% at 500 °C to 95% at 750 °C. The high selectivity of ethylene and propylene at high temperatures was mainly due to the intensification of the monomolecular cracking reaction. After 20 times of regeneration, the acidity and pore structure of the zeolite had hardly changed, and the conversion of pentene remained above 80% at 650 °C.

**Keywords:** pentene; catalytic cracking; ethylene; propylene



**Citation:** Han, Y.; Du, L.; Zhu, Y.; Xu, Y.; Bai, X.; Ouyang, Y.; Luo, Y.; Shu, X. High-Temperature Cracking of Pentene to Ethylene and Propylene over H-ZSM-5 Zeolites: Effect of Reaction Conditions and Mechanistic Insights. *Catalysts* **2023**, *13*, 73. <https://doi.org/10.3390/catal13010073>

Academic Editors: Luísa Margarida Martins, Maria Luisa Di Gioia and Isidro M. Pastor

Received: 3 December 2022

Revised: 21 December 2022

Accepted: 26 December 2022

Published: 30 December 2022



**Copyright:** © 2022 by the authors. Licensee MDPI, Basel, Switzerland. This article is an open access article distributed under the terms and conditions of the Creative Commons Attribution (CC BY) license (<https://creativecommons.org/licenses/by/4.0/>).

## 1. Introduction

Light olefins such as ethylene and propylene are key building blocks of the chemical industry, and demand for them has been increasing year by year [1]. The forecast demand of propylene is expected to average 4.3% per year in the next decade according to IHS Markit [2]. At present, light olefins are mainly produced by steam cracking of naphtha. The traditional technologies of producing light olefins cannot meet the market demand [3]. On the other hand, with the popularity of new energy vehicles, gasoline consumption is expected to decrease in the future [4,5]. China's gasoline demand is expected to reach its maximum in 2022 [6]. Therefore, the study on converting gasoline to light olefins has attracted more and more attention from researchers. Since the olefins in fluid catalytic cracking (FCC) gasoline are up to 30–65 vol% [7], olefin cracking of FCC gasoline can relieve the pressure of gasoline surplus and also make up for the shortage of light olefins [8]. Recently, our team proposed an FCC process for targeted cracking of light olefins [9]. The key to this process is to maximize the cracking of olefin in FCC gasoline to ethylene and propylene. As the main olefin component in FCC gasoline, pentene is often selected as a model compound to study the FCC gasoline cracking reaction.

For the mechanism of pentene cracking over acidic zeolites, it is generally believed that monomolecular (protolytic) and bimolecular (oligomerization cracking) pentene cracking are the main reaction pathways [10,11]. Lin et al. [12] established cracking routes of pentene, as shown in Figure 1. The selectivity of ethylene and propylene can be promoted by controlling the reaction pathway. Miyaji et al. [13] reported that when the spatial volume of the zeolite cavity was almost the same as the volume of pentyl cations, the high selectivity of ethylene and propylene was obtained via strengthening monomolecular cracking of

pentene. Lin et al. [12] studied the effect of acid strength on the cracking reaction of pentene. They concluded that strong acid sites could promote the reaction pathways that produced ethylene, while weak acid sites preferred the reaction pathways that formed propylene. Sun et al. [8] found that a high strong Brønsted acid site concentration was conducive to the monomolecular cracking of pentene and could improve the total yield of ethylene and propylene. In these studies, the selectivity of ethylene and propylene was improved by adjusting the zeolite properties and controlling the reaction pathway. In addition, reaction conditions, especially temperature, can also significantly affect the pentene reaction pathway and the selectivity of ethylene and propylene [10].

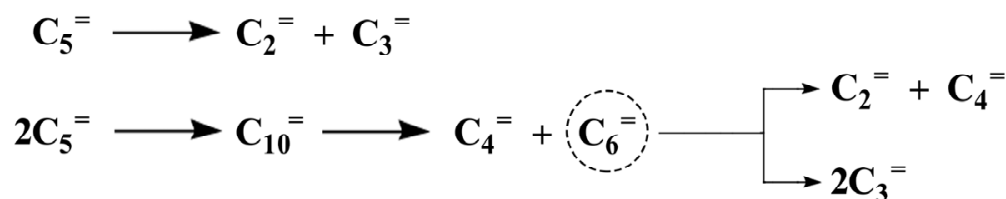


**Figure 1.** Reaction routes of pentene mono- and bimolecular cracking.

Zhu et al. [14] investigated the effect of reaction conditions on the cracking of butene to ethylene and propylene. They found that the ethylene selectivity increased gradually with increased temperature and decreased WHSV, while the propylene selectivity increased first and then decreased. Chen et al. [15] and Sun et al. [16] studied the reaction of hexene to ethylene and propylene under various conditions and obtained similar conclusions. Some studies have reported the effect of temperature on the pentene cracking reaction [17–25]. Huang et al. [18] studied the kinetics of C<sub>3</sub>–C<sub>7</sub> olefin transformation. They found that the monomolecular cracking reaction of pentene had a high activation energy. The rate of monomolecular cracking increased with rising temperature, while that of bimolecular cracking fell. Therefore, the selectivity of ethylene and propylene was strengthened with the increase in temperature. Aretin et al. [19] established a single-event kinetic model for 1-pentene cracking on H-ZSM-5 and obtained similar conclusions. Zhang et al. [22] studied the thermodynamic equilibrium distribution of the olefin catalytic pyrolysis process. They found that the thermodynamic equilibrium composition of ethylene and propylene was 10% and 30% at 550 °C up to 50% and 40% at 750 °C, respectively. Thus, in order to improve the yield of ethylene and propylene, it was necessary to increase the reaction temperature. As for pentene cracking at high temperatures (>600 °C), the reaction modes include thermal cracking following the free radical mechanism [26,27] and catalytic cracking following the carbenium ion mechanism [28,29].

Previous studies about pentene cracking reactions mainly focused on 500–600 °C (in this temperature range, the thermal cracking reaction is insignificant). It is still a much-disputed subject whether the pentene cracking reaction mainly follows a thermal or catalytic cracking mechanism at high temperatures (>600 °C). This study aims to explore the roles of thermal cracking and catalytic cracking reaction for pentene cracking over H-ZSM-5 at high temperatures (>600 °C). Therefore, a thermal/catalytic cracking proportion model was established based on the analysis of pentene cracking over H-ZSM-5 and quartz sand at different temperatures. We found that the proportion of pentene feed chemically adsorbed with the acid sites and cracked through catalytic cracking was above 88.4%, even at 750 °C. In addition, the reason for the high ethylene and propylene selectivity of pentene was elucidated by deducing and estimating the cracking pathway at high temperatures. These results are of reference value for optimizing reaction conditions and understanding the reaction mechanism of pentene cracking at high temperatures.

## 2. Results

### 2.1. Pentene Cracking Reaction over H-ZSM-5 with Different Conditions

#### 2.1.1. Effect of Reaction Temperature on the Yields and Selectivities of Pentene Cracking Products

The effect of reaction temperature on the main product yields (a) and selectivities (b) from pentene cracking are shown in Figure 2. As shown in Figure 2a, the total yield of ethylene and propylene reached a maximum (60.1%) at 700 °C. In Figure 2b, the ethylene selectivity increased with increasing temperature, and the propylene selectivity reached a maximum at 700 °C, while the butene selectivity decreased with increasing temperature. Some researchers observed similar trends for the effect of reaction temperature on the product selectivity in the pentene cracking reaction at 250–550 °C [18,19,25].

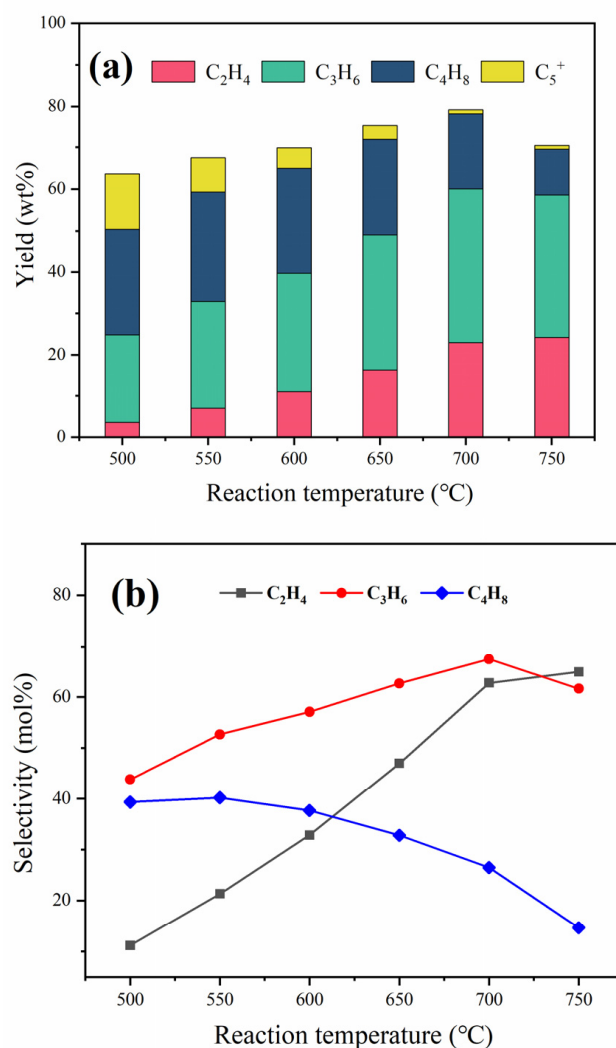


**Figure 2.** The main product yields (a) and selectivities (b) from pentene cracking over H-ZSM-5 vs. reaction temperatures. (C<sub>5</sub><sup>+</sup> fraction is defined as C<sub>6</sub>–C<sub>10</sub> hydrocarbon which does not include aromatics). Reaction conditions: total pressure, 130 kPa; partial pressure, 60 kPa; WHSV, 83 h<sup>−1</sup>.

As shown in Figure 1, butene originates from a bimolecular cracking reaction. The decrease in butene selectivity indicated that high temperatures inhibited the bimolecular cracking reaction. This effect of increasing temperature to restrain the bimolecular cracking of pentene has been previously reported in the literature [12,16,18,19]. The propylene selectivity first went up and then went down. This was because, to a certain extent, the high temperature enhanced the cracking rate so as to improve the propene selectivity. However, at a certain temperature, the aromatization reaction would aggravate and re-

duce the propene selectivity. This is consistent with the research of Chen et al. [15] and Kubo et al. [30].

Figure 3 shows the selectivities of byproducts from pentene cracking over H-ZSM-5 at different reaction temperatures. The selectivities of H<sub>2</sub> and CH<sub>4</sub> + C<sub>2</sub>H<sub>6</sub> increased markedly with increasing temperature, while the selectivity of the C<sub>3</sub>–C<sub>5</sub> paraffin decreased sharply. The total aromatics selectivity decreased slowly and then increased gradually. H<sub>2</sub> was mainly derived from the dehydrogenation reaction. The increase in H<sub>2</sub> selectivity indicated that the high temperature favored the dehydrogenation reaction. The increase in CH<sub>4</sub> + C<sub>2</sub>H<sub>6</sub> selectivity might be related to the acceleration of the thermal cracking [16]. The decrease in C<sub>3</sub>–C<sub>5</sub> paraffin selectivity was attributed to the inhibition of the hydrogen transfer reaction by the high temperatures [14]. The process of aromatics formation in olefin cracking reactions is generally believed to proceed through the cyclization of olefins, followed by hydrogen transfer or a dehydro-aromatization reaction [12,31]. Choudhary et al. [32] reported that the aromatization reaction involved mainly hydrogen transfer reactions at lower temperatures, but it involved mainly dehydro-aromatization reactions at higher temperatures. The possible reason for the non-monotonic variation of total aromatic selectivity with increasing temperature was that the aromatics generated by the hydrogen transfer reaction decreased, while those generated by the dehydro-aromatization reaction increased. The variation trend of the total aromatic selectivity was consistent with C<sub>3</sub>–C<sub>5</sub> paraffin selectivity at 500–600 °C and consistent with H<sub>2</sub> selectivity at 650–750 °C, which confirmed the view above. Chen et al. [33] observed a similar trend for the effect of reaction temperature on aromatics formation.

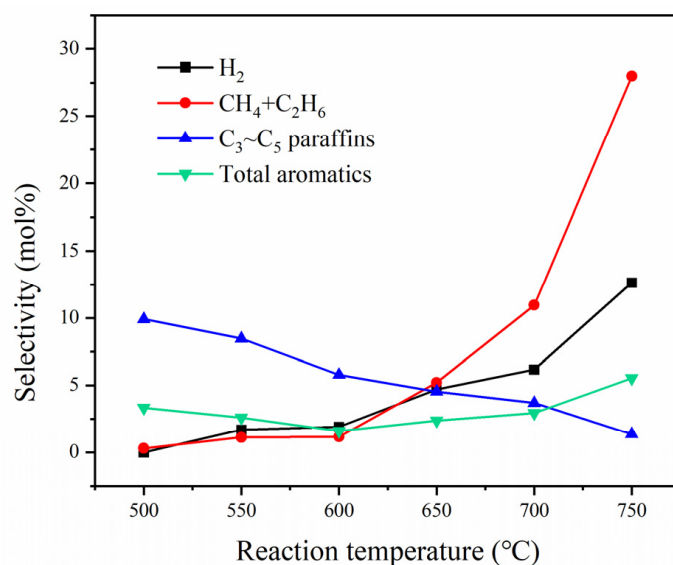


**Figure 3.** Selectivities of byproducts from pentene cracking over H-ZSM-5 vs. reaction temperatures. Reaction conditions: total pressure, 130 kPa; partial pressure, 60 kPa; WHSV, 83 h<sup>-1</sup>.

### 2.1.2. Effect of WHSV on the Yields and Selectivities of Pentene Cracking Products

The effects of WHSV on the main product yields (a) and selectivities (b) of pentene cracking over H-ZSM-5 are shown in Figure 4. As shown in Figure 4a, the total yield of ethylene and propylene reached a maximum (67.8%) at 57 h<sup>-1</sup>. In Figure 4b, with the increase in WHSV, the ethylene selectivity decreased while the butene selectivity increased. The reason for this variation may be that the secondary cracking of butene is enhanced at low WHSV. Propylene selectivity increased first and then decreased with increasing WHSV. This was because low WHSV would aggravate the long-chain olefins such as C<sub>5</sub><sup>+</sup> olefins cracking to propylene and accelerate the aromatization and hydrogen transfer reaction of propylene; however, high WHSV made the cracking reaction insufficient [15].

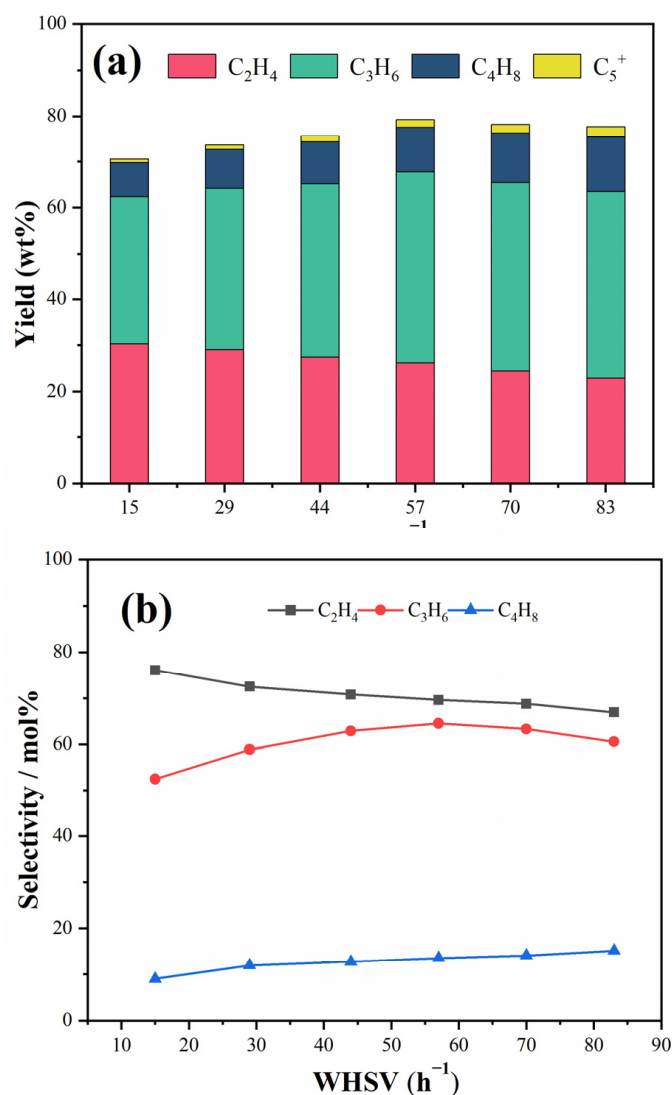


**Figure 4.** The main product yields (a) and selectivities (b) of pentene cracking over H-ZSM-5 vs. WHSV. (C<sub>5</sub><sup>+</sup> fraction is defined as C<sub>6</sub>–C<sub>10</sub> hydrocarbon which does not include aromatics) Reaction conditions: total pressure, 130 kPa; partial pressure, 60 kPa; reaction temperature, 700 °C.

The effects of WHSV on the selectivities of byproducts from pentene cracking over H-ZSM-5 are shown in Figure 5. The selectivities of H<sub>2</sub>, CH<sub>4</sub> + C<sub>2</sub>H<sub>6</sub>, and total aromatics decreased markedly with increasing WHSV, whereas the selectivity of the C<sub>3</sub>–C<sub>5</sub> paraffin increased marginally and then decreased gradually. The variation trends of H<sub>2</sub> and total aromatics selectivity were consistent, indicating that the aromatics were mainly derived from dehydro-aromatization reaction under such conditions, and low WHSV promoted this reaction. This result is consistent with the previous research by Choudhary et al. [34]. The drop in the selectivity of CH<sub>4</sub> + C<sub>2</sub>H<sub>6</sub> might be due to the high WHSV inhibiting the thermal cracking. The C<sub>3</sub>–C<sub>5</sub> paraffin selectivity varied non-monotonically because the increase in WHSV promoted the selectivity of C<sub>3</sub>–C<sub>5</sub> olefin, and the formation of C<sub>3</sub>–C<sub>5</sub> paraffin resulted from C<sub>3</sub>–C<sub>5</sub> olefin [35]; simultaneously, the inhibition of the hydrogen transfer reaction by the high WHSV suppressed the selectivity of the C<sub>3</sub>–C<sub>5</sub> paraffin [15].

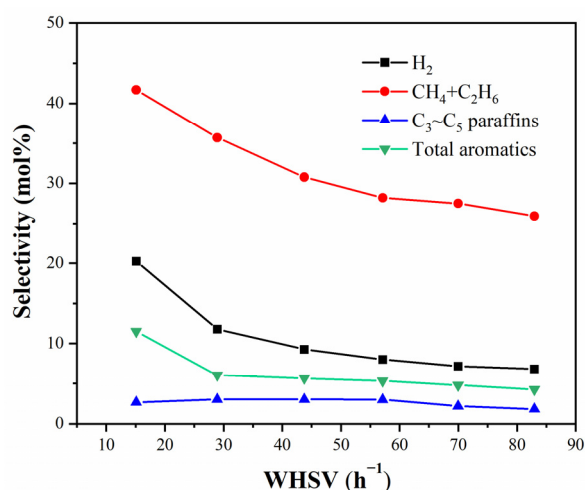


**Figure 5.** Selectivities of byproducts from pentene cracking over H-ZSM-5 vs. WHSV. Reaction conditions: total pressure, 130 kPa; partial pressure, 60 kPa; reaction temperature, 700 °C.

## 2.2. Roles of Thermal Cracking and Catalytic Cracking in Pentene Cracking over H-ZSM-5 at High Temperatures

The modes for pentene cracking over H-ZSM-5 at high temperatures include thermal cracking following the free radical mechanism [26] and catalytic cracking following the carbenium ion mechanism [28]. In order to clarify the roles of thermal cracking and catalytic cracking, comparative experiments were performed over quartz sand and H-ZSM-5.

As shown in Figure 6, the conversion of pentene cracking over quartz sand was negligible at 500–600 °C. Therefore, the thermal cracking reaction in this temperature range was no longer considered. Then, with the growth of temperature, the conversion gradually increased. Obviously, the thermal cracking reaction cannot be ignored when the temperature exceeds 600 °C, so the catalytic cracking and thermal cracking reactions coexist for the pentene cracking over H-ZSM-5 at 650–750 °C. Moreover, the conversion of pentene cracking over quartz sand at 650–750 °C was lower than 50%; however, the conversion over H-ZSM-5 exceeded 80% at 500–600 °C. Therefore, it could be inferred that the conversion of pure catalytic cracking was higher than that of thermal cracking across the whole temperature range.

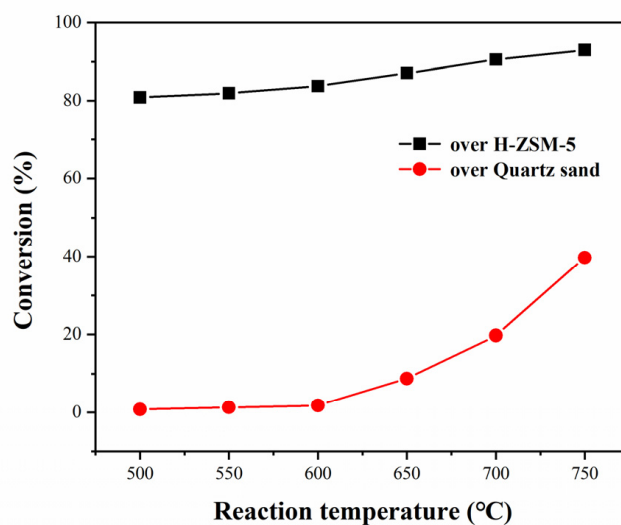


**Figure 6.** Conversions of pentene cracking over quartz sand and H-ZSM-5 vs. reaction temperatures. Reaction conditions: total pressure, 130 kPa; partial pressure, 60 kPa; WHSV, 83 h<sup>-1</sup>.

In order to quantify the magnitude of the thermal cracking and the catalytic cracking for pentene cracking over H-ZSM-5 at 650–750 °C, a thermal/catalytic cracking proportion model was established. The scheme of the model is shown in Figure 7.

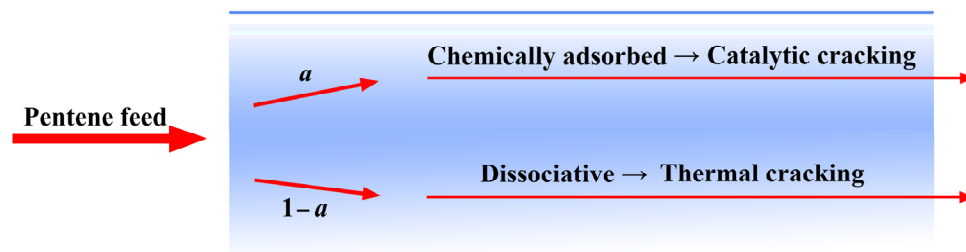


**Figure 7.** The thermal/catalytic cracking proportion model for pentene cracking over H-ZSM-5.

As far as we know, this is the first time that the model has been proposed and applied to the olefin cracking reaction at high temperatures. For a certain amount of pentene reactant in the reaction, the portion chemically adsorbed with the acid sites was accounted for  $a$ , which was supposed to be catalytically converted or finally desorbed; the remaining portion was dissociative and accounted for  $1 - a$ , which was supposed to be thermally cracked or unreacted. Therefore, the total conversion of pentene over H-ZSM-5 at 650–750 °C could be expressed as Equation (1):

$$a \times C_{\text{catalytic}} + (1 - a) \times C_{\text{thermal}} = C_{\text{total}} \quad (1)$$

where  $C_{\text{catalytic}}$  is the conversion of catalytic cracking for chemically adsorbed pentene,  $C_{\text{thermal}}$  is the conversion of thermal cracking for dissociative pentene, and  $C_{\text{total}}$  is the total conversion for pentene feed.

Equation (1) can be transformed into Equation (2).

$$a = (C_{\text{total}} - C_{\text{thermal}}) / (C_{\text{catalytic}} - C_{\text{thermal}}) \quad (2)$$

$C_{\text{catalytic}}$  is greater than  $C_{\text{total}}$ , because  $a$  is less than one. This is consistent with the conclusion from Figure 6. In Equation (2),  $C_{\text{thermal}}$  and  $C_{\text{total}}$  are observed values from the experiments of the pentene cracking reaction over quartz sand and H-ZSM-5, respectively. The value of  $C_{\text{catalytic}}$  is not measurable at 650–750 °C because thermal cracking and catalytic cracking coexist. However, the value ranges of  $C_{\text{catalytic}}$  can be deduced from  $C_{\text{total}}$ . For example, the  $C_{\text{total}}$  is 87.1% (Figure 6) at 650 °C; therefore, the value range of  $C_{\text{catalytic}}$  is 87.1–100%. Moreover, the values of  $C_{\text{thermal}}$ ,  $C_{\text{catalytic}}$ ,  $C_{\text{total}}$ , and  $a$  are all fixed under certain reaction conditions. Therefore, substituting the maximum possible value of  $C_{\text{catalytic}}$  into Equation (2), the minimum possible value of  $a$  can be obtained. For example, the value range of  $C_{\text{catalytic}}$  is 87.1–100% at 650 °C; therefore, the value range of  $a$  is 85.9–100%. The value ranges of  $C_{\text{catalytic}}$  and  $a$  at 650–750 °C are shown in Table 1. As shown in Table 1, the proportion of pentene feed chemically adsorbed with the acid sites is more than 85.8% at 650–750 °C, and these pentenes converted via catalytic cracking are more than 87.1%. It indicates that the catalytic cracking dominates the global cracking reaction even at 750 °C.

**Table 1.** Value ranges of  $C_{\text{catalytic}}$  and  $a$  in pentene cracking over H-ZSM-5 at 650–750 °C and 83 h<sup>−1</sup>.

Reaction Temperature, °C	$C_{\text{catalytic}}$	$a$
650	87.1–100%	85.8–100%
700	91.6–100%	89.5–100%
750	93.0–100%	88.4–100%

The yield of each product from the thermal cracking reaction can be estimated by Equation (3) when pentene reacts over H-ZSM-5 at 650–750 °C.

$$y_{i,\max} = (1 - a_{\min}) \times y_{\text{thermal},i} \quad (3)$$

where  $y_{i,\max}$  is the maximum yield of the product  $i$  from thermal cracking of pentene cracking over H-ZSM-5, and  $y_{\text{thermal},i}$  is the yield of the product  $i$  from pentene cracking over quartz sand.

The product distributions of pentene cracking over quartz sand at various temperatures are listed in Table S1 (in the Supplementary Materials). As shown in Table S1, the main products of thermal cracking are methane, ethane, ethylene, propylene, and butene. Figure 8 shows the proportion of the main products derived from catalytic cracking and thermal cracking for pentene cracking over H-ZSM-5 at 650–750 °C. The contribution of the thermal cracking reaction to each product was calculated by Equation (3).

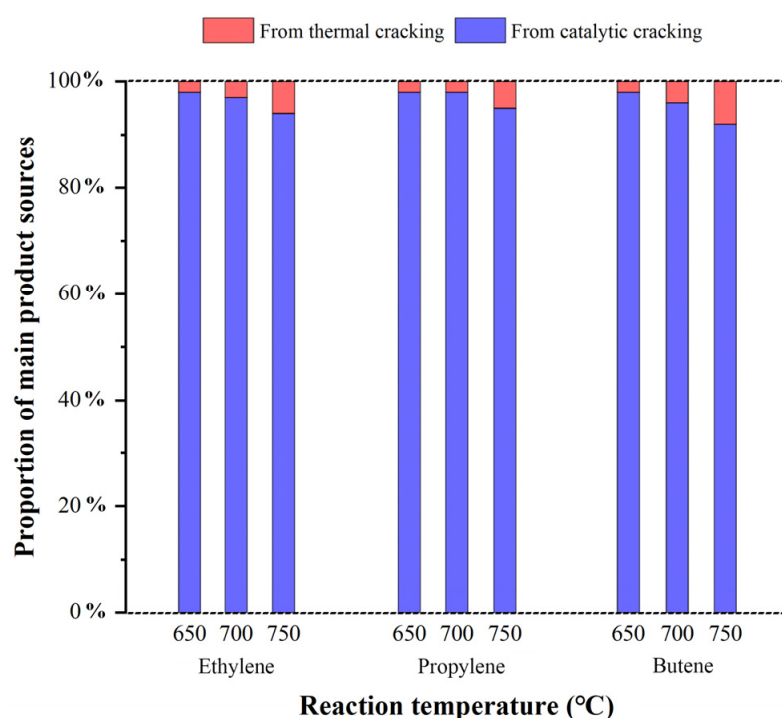


**Figure 8.** The proportion of the main products derived from catalytic cracking and thermal cracking for pentene cracking over H-ZSM-5 at 650–750 °C. Reaction conditions: total pressure, 130 kPa; partial pressure, 60 kPa; WHSV, 83 h<sup>-1</sup>.

As shown in Figure 8, with increasing temperature, the contribution of the thermal cracking reaction to the main products gradually increased. However, even at 750 °C, the contribution of thermal cracking to ethylene, propylene, and butene was less than 10%. This indicated that the light olefins in the products were mainly derived from catalytic cracking rather than thermal cracking, even at 750 °C. Hou et al. [36] obtained a different result in the C<sub>5</sub> alkane cracking reaction over ZSM-22 at high temperatures. They found that C<sub>5</sub> alkane mainly followed the thermal cracking reaction mechanism at 700–800 °C.

The proportion of methane and ethane derived from catalytic cracking and thermal cracking for pentene cracking over H-ZSM-5 at 650–750 °C is shown in Figure 9.

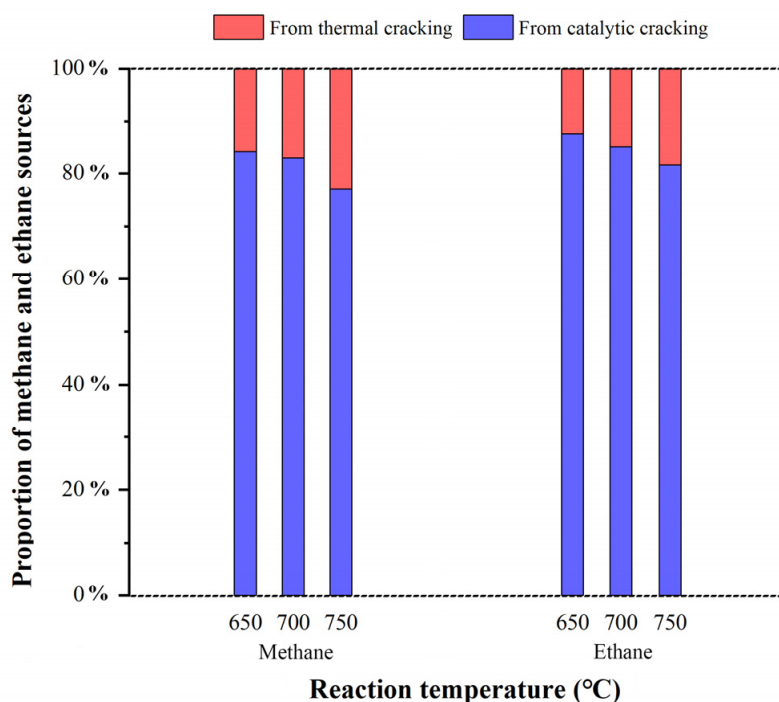


**Figure 9.** The proportion of methane and ethane derived from catalytic cracking and thermal cracking for pentene cracking over H-ZSM-5 at 650–750 °C. Reaction conditions: total pressure, 130 kPa; partial pressure, 60 kPa; WHSV, 83 h<sup>-1</sup>.

As shown in Figure 9, the proportion of methane and ethane derived from thermal cracking increased with increasing temperature, while the contribution of thermal cracking to methane and ethane was less than 30% even at 750 °C. Therefore, it can be concluded that methane and ethane mainly arise from catalytic cracking but not thermal cracking. Longstaff [37] found that methane and ethane were mainly derived from catalytic cracking rather than thermal cracking reactions for naphtha cracking at 650 °C over ZSM-5.

The pentene molecule contains an electron-rich structure of a carbon–carbon double bond, which is very easily chemically adsorbed at the acid site of H-ZSM-5 zeolite to form a carbenium ion [38,39]. The fast chemical adsorption of pentene feed resulted in a sharp decrease in dissociative pentene feed. Once the carbenium ion intermediate was formed, it was more challenging to undergo a thermal cracking reaction because the presence of a positive charge resulted in the electrons in the carbon–carbon bonds shifting, making it hard to homogenize and form free radicals. Castro-Marcano et al. [40] found that the formation of unstable methyl and ethyl carbenium ion intermediates became possible at high temperatures, and methane and ethane could arise from the hydrogen transfer reaction of methyl and ethyl carbenium ions.

### 2.3. Deduction and Estimation of Reaction Pathways for Pentene Catalytic Cracking

As proven in Section 2.2, the pentene cracking reaction is mainly via catalytic cracking rather than thermal cracking, even at 650–750 °C. Some useful information about pentene cracking pathways can be obtained based on product distribution.

The paraffin in the cracking product is derived from the hydrogen transfer reaction of the olefin with the same carbon number [41]. Therefore, pentene cracking pathways could be estimated based on the carbon balance. Table 2 shows the selectivities of the main product from pentene catalytic cracking reaction at different temperatures over H-ZSM-5. The products from the thermal cracking reaction have been deduced by using Equation (3).

**Table 2.** Selectivities of the main product from pentene catalytic cracking under various temperatures. Reaction conditions: total pressure, 130 kPa; partial pressure, 60 kPa; WHSV, 83 h<sup>-1</sup>.

Reaction Temperature, °C	Product Selectivity, mol%			
	C <sub>1</sub> <sup>a</sup>	C <sub>2</sub> <sup>b</sup>	C <sub>3</sub> <sup>c</sup>	C <sub>4</sub> <sup>d</sup>
500	trace	11.33	46.69	44.17
550	trace	21.79	56.05	44.58
600	trace	33.23	58.90	38.75
650	2.31	47.77	63.56	33.85
700	5.71	64.61	68.92	26.65
750	14.39	69.32	60.30	13.74

<sup>a</sup> C<sub>1</sub> represents the selectivity of methane; <sup>b</sup> C<sub>2</sub> represents the total selectivity of ethane plus ethylene; <sup>c</sup> C<sub>3</sub> represents the total selectivity of propane plus propylene; <sup>d</sup> C<sub>4</sub> represents the total selectivity of butane plus butene.

As shown in Table 2, a large amount of methane was generated by catalytic cracking reactions at 650–750 °C. Buchanan et al. [42] proposed that methane can arise from the methyl carbenium ion, followed by the hydrogen transfer reaction. Castro-Marcano et al. [40] confirmed that the methyl carbenium ion could exist at high temperatures, and methane could be produced by the hydrogen transfer reaction of methyl carbenium ion by molecular dynamics simulation.

In general, bimolecular cracking of pentene was unfavorable for the formation of ethylene [12,18]. Moreover, even in monomolecular cracking of pentene, C<sub>2</sub> selectivity should be the same as that of C<sub>3</sub>, and C<sub>1</sub> selectivity should be equal to that of C<sub>4</sub>. However, the C<sub>2</sub> selectivity was higher than that of C<sub>3</sub>, and the C<sub>1</sub> selectivity was higher than that of C<sub>4</sub> at 750 °C. The reasonable explanation for this phenomenon might be that part of the butene in the product underwent secondary cracking.

The bimolecular cracking process dominates at low temperatures [17], which is not conducive to forming the methyl carbenium ion. Hence, the pathways of generating methyl carbenium ions in the whole bimolecular cracking process were ignored. Moreover, in bimolecular cracking, C<sub>10</sub> carbenium ions had more energetically favorable β-scission modes available [42]. Thus, neglecting their direct cracking to the ethyl carbenium ion or ethylene is reasonable.

Based on the analysis above, the possible cracking pathways of pentene are summarized in Figure 10. As shown in Figure 10, the cracking reaction follows pathway I (C<sub>5</sub><sup>+</sup> → C<sub>1</sub> + C<sub>4</sub><sup>+</sup>), pathway II (C<sub>5</sub><sup>+</sup> → C<sub>2</sub><sup>+</sup> + C<sub>3</sub><sup>+</sup>), and pathway III (2C<sub>5</sub><sup>+</sup> → C<sub>10</sub><sup>+</sup>). Because C<sub>10</sub><sup>+</sup> can further crack into light olefins, pathway III has four subsequent branches: pathway III-1 (C<sub>10</sub><sup>+</sup> → C<sub>4</sub><sup>+</sup> + C<sub>6</sub><sup>+</sup> → C<sub>2</sub><sup>+</sup> + 2C<sub>4</sub><sup>+</sup>), pathway III-2 (C<sub>10</sub><sup>+</sup> → C<sub>4</sub><sup>+</sup> + C<sub>6</sub><sup>+</sup> → 2C<sub>3</sub><sup>+</sup> + C<sub>4</sub><sup>+</sup>), pathway III-3 (C<sub>10</sub><sup>+</sup> → C<sub>3</sub><sup>+</sup> + C<sub>7</sub><sup>+</sup> → 2C<sub>3</sub><sup>+</sup> + C<sub>4</sub><sup>+</sup>), and pathway III-4 (C<sub>10</sub><sup>+</sup> → C<sub>3</sub><sup>+</sup> + C<sub>7</sub><sup>+</sup> → C<sub>2</sub><sup>+</sup> + C<sub>3</sub><sup>+</sup> + C<sub>5</sub><sup>+</sup>). It is noteworthy that pathway I can only proceed above 650 °C, and the secondary cracking of butene can only occur at 750 °C.

According to the main cracking pathways in Figure 10, some essential estimations can be made. We assumed that pathway III accounted for *b*, pathway II accounted for *c*, and pathway I accounted for 1 − *b* − *c*. The possibility of pathway III-4 was ignored because it was negligible compared with the other reaction pathways [12,13]. For the conversion of the C<sub>10</sub> carbenium ion intermediates, pathway III-1 was assumed to account for *d*; pathways III-2 and III-3 having the same final products totally accounted for 1 − *d*. Without considering the secondary cracking of butene, it can be assumed that C<sub>1</sub>/C<sub>2</sub> = (1 − *b* − *c*)/(*c* + 0.5*bd*), C<sub>2</sub>/C<sub>3</sub> = (*c* + 0.5*bd*)/(*c* + *b* − *bd*), C<sub>3</sub>/C<sub>4</sub> = (*c* + *b* − *bd*)/(1 − 0.5*b* − *c* + 0.5*bd*). Lin et al. [12] used a similar method to estimate the cracking reaction pathway of 1-pentene. Methane selectivity was negligible at 500–600 °C (Table 2). Therefore, 1 − *b* − *c* = 0 was observed in this temperature range. At 750 °C, the secondary cracking proportion in the generated butene accounted for *k*. At this point, *b* was obtained by extrapolating its value at 500–700 °C (Figure 11). The values of *b*, *c*, and *d* can be calculated according to the selectivity of C<sub>1</sub>–C<sub>4</sub> (Table 2).

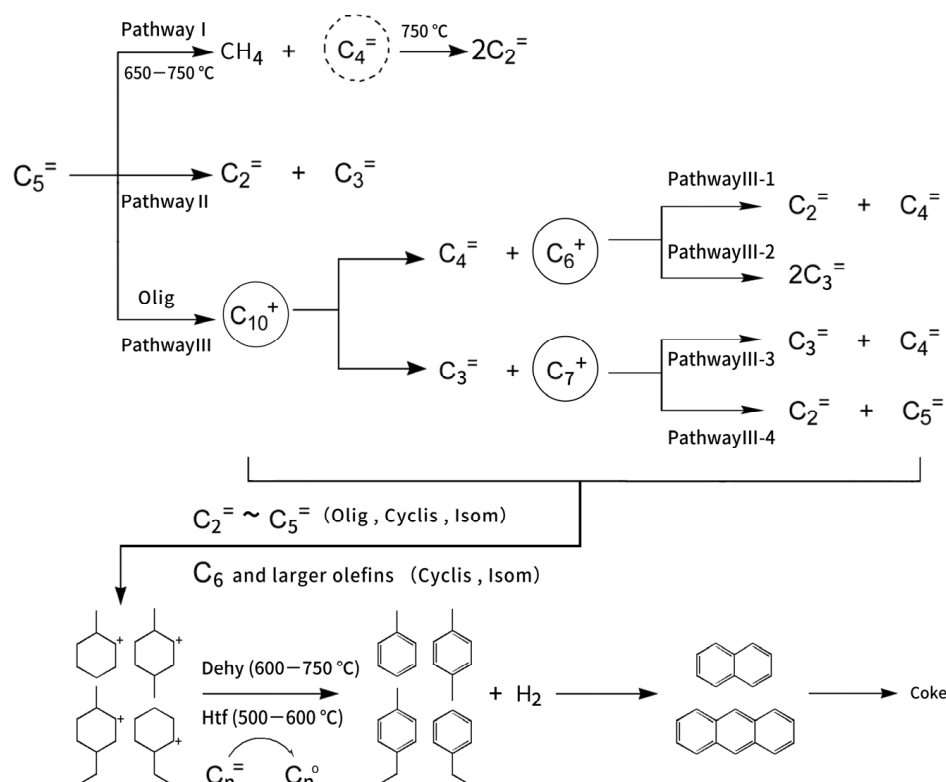


**Figure 10.** Possible cracking pathways of pentene (full line circle represents all cracking, dotted line circle represents part cracking).

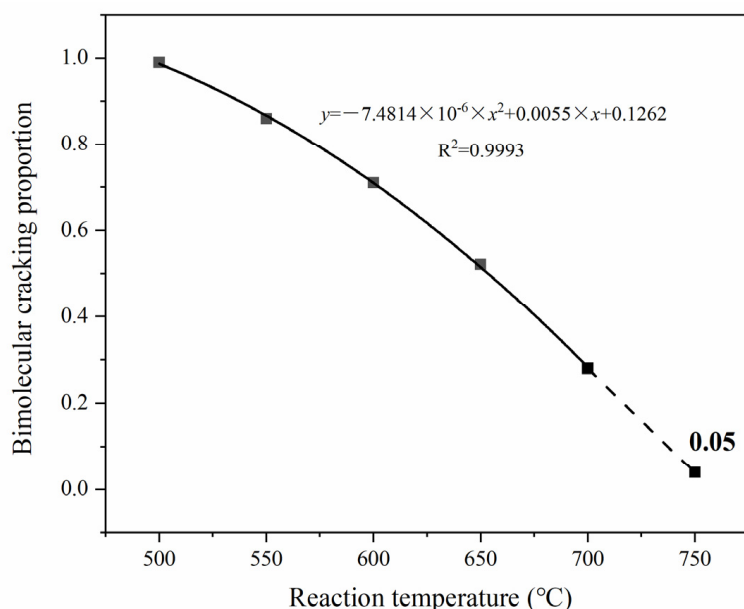


**Figure 11.** Bimolecular cracking proportions of pentene vs. reaction temperatures. Reaction conditions: total pressure, 130 kPa; partial pressure, 60 kPa; WHSV, 83 h<sup>-1</sup>.

Table 3 shows the cracking pathway proportions of pentene under various temperatures. As shown in Table 3, the proportion of pathway III decreased from 99% at 500 °C to 5% at 750 °C, indicating that high temperatures suppressed the bimolecular cracking reaction. However, the proportions of pathway II and pathway III-1 increased with increasing temperature, suggesting that increasing temperature favored the pathways of ethylene formation. Notably, although the proportion of pathway III-1 to the total bimolecular

cracking pathways increased, the ratio of bimolecular cracking to total pentene cracking decreased rapidly. Therefore, pathway III-1 was not the primary source of ethylene at high temperatures. In addition, the proportion of pathway I gradually increased from 650 °C to 750 °C, and 23% of butene underwent secondary cracking at 750 °C to ethylene. These results showed that the increase in ethylene selectivity was mainly caused by pathway II and the secondary cracking of butene.

**Table 3.** Cracking pathway proportions of pentene under various temperatures. Reaction conditions: total pressure, 130 kPa; partial pressure, 60 kPa; WHSV, 83 h<sup>-1</sup>.

Reaction Temperature, °C	Cracking Pathway Proportions				
	<i>b</i>	<i>c</i>	1 - <i>b</i> - <i>c</i>	<i>d</i>	<i>k</i>
500	0.99	0.01	0.00	0.32	-
550	0.86	0.14	0.00	0.33	-
600	0.71	0.29	0.00	0.37	-
650	0.52	0.45	0.03	0.42	-
700	0.30	0.64	0.06	0.56	-
750	0.05	0.76	0.19	0.79	0.23

#### 2.4. Regeneration Performance of the Zeolite

The regeneration experiments of H-ZSM-5 zeolite were carried out to investigate its regeneration performance. The cracking reaction of pentene was carried out at 650 °C and 83 h<sup>-1</sup> then the zeolite was regenerated. The conversion, ethylene yield, and propylene yield were selected as indexes. As shown in Figure 12, the conversion, ethylene yield, and propylene yield had little change. After 20 times of regeneration, the conversion of pentene was still greater than 80%, and the yield of ethylene and propylene was greater than 15% and 30%, respectively. It showed that H-ZSM-5 zeolite had a good regeneration performance.

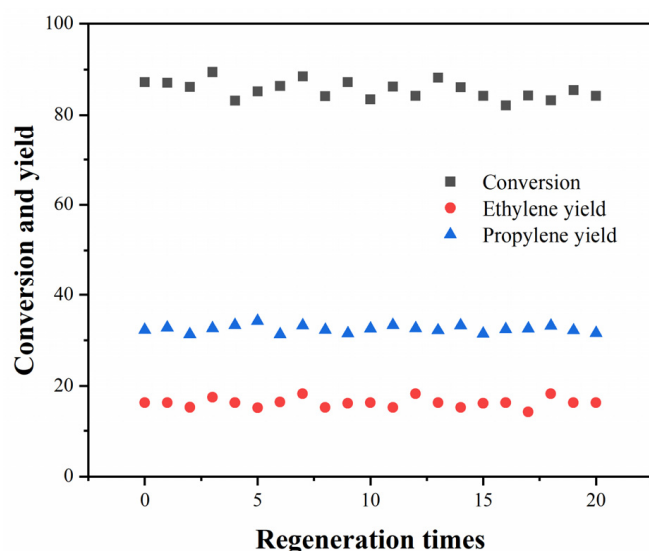


**Figure 12.** Regeneration performance evaluation of H-ZSM-5 zeolite. Reaction conditions: total pressure, 130 kPa; partial pressure, 60 kPa; 650 °C; WHSV, 83 h<sup>-1</sup>. Regeneration conditions: 670 °C; Compressed air (120 mL·min<sup>-1</sup>) sweeps for 10 min.

Figure 13 shows the XRD pattern of H-ZSM-5 before and after 20 times of regeneration. It can be seen from Figure 13 that the peak position and diffraction intensity of the zeolite after 20 times of regeneration are completely consistent with the fresh zeolite, indicating that the skeleton structure of H-ZSM-5 zeolite has not changed after multiple reactions and regenerations.

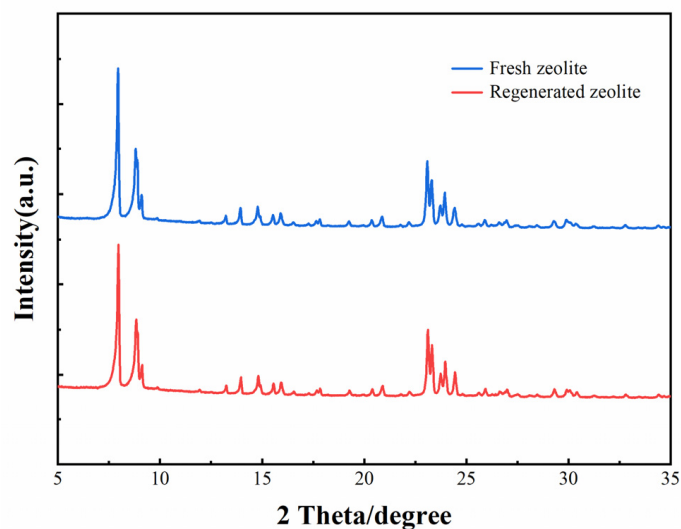


Figure 13. XRD pattern of fresh and regenerated HZSM-5 zeolite.

The acid strength of the fresh, regenerated, and spent zeolites was determined by  $\text{NH}_3$ -TPD, as shown in Figure 14. The TPD profiles showed a similar peak position and size for the fresh and regenerated zeolite, indicating that the acid properties after regeneration had barely changed. However, the TPD profiles of spent zeolite differed from the former. The weak acid peak (at around 210 °C) of the spent zeolite was smaller than the fresh zeolite, and the strong acid peak almost did not exist. This showed that the deactivation of the zeolite had a more significant effect on the strong acid site.

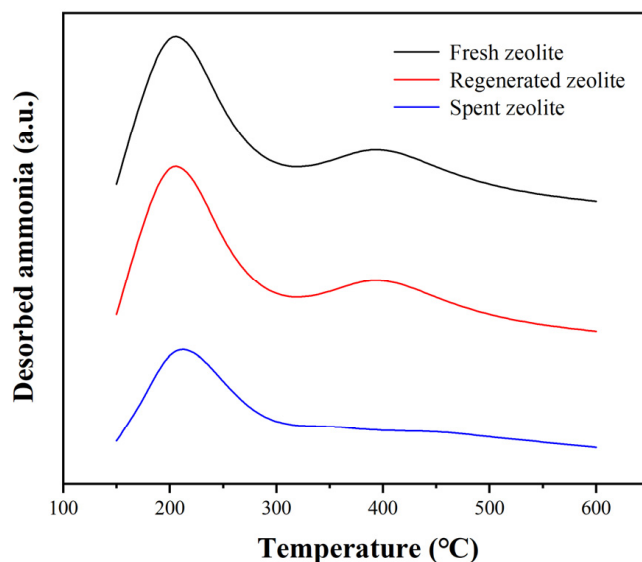


Figure 14. The  $\text{NH}_3$ -TPD profiles of fresh, regenerated, and spent HZSM-5 zeolite.

In Table 4, the surface area and pore volume of fresh, regenerated, and spent catalysts were measured by BET, while FTIR was used to measure the acid concentration. There was no obvious difference in these properties between fresh and regenerated zeolite, indicating that the properties of zeolite did not change after regeneration. However, the surface area, pore volume, and acid concentration of the spent catalyst were smaller than fresh zeolite, especially the micropore area, micropore volume, and Brønsted acid concentration. This showed that the deactivation of the zeolite mainly affected the microporous structure and Brønsted acid site of the zeolite.

**Table 4.** Textural properties of the H-ZSM-5.

Zeolite	Surface Area (m <sup>2</sup> ·g <sup>-1</sup> ) <sup>a</sup>		Pore Volume (cm <sup>3</sup> ·g <sup>-1</sup> ) <sup>a</sup>		Acid Concentration (μmol·g <sup>-1</sup> ) <sup>b</sup>	
	Total	Micro	Total	Micro	LAS	BAS
Fresh zeolite	366	334	0.192	0.171	116.1	27.1
Regenerated zeolite	352	322	0.185	0.162	113.3	25.2
Spent zeolite	301	284	0.152	0.139	52.3	2.5

<sup>a</sup> Detected by BET; <sup>b</sup> Derived from FT-IR spectroscopy with pyridine as a probe molecule.

### 3. Materials and Methods

#### 3.1. Feedstock and Catalyst Preparation

1-Pentene was purchased from Tokyo Chemical Industry (Shanghai) Co., Ltd. (Tokyo, Japan) with a purity higher than 98%. We found that the conversion and ethylene/propylene selectivity of pentene cracking over the aged H-ZSM-5 zeolite with an SiO<sub>2</sub>/Al<sub>2</sub>O<sub>3</sub> ratio of about 100 was a good compromise. The H-ZSM-5 zeolite powder (*n*(SiO<sub>2</sub>):*n*(Al<sub>2</sub>O<sub>3</sub>) = 95.6) was purchased from the Sinopec Catalyst Corporation of China (Beijing). Diammonium hydrogen phosphate ((NH<sub>4</sub>)<sub>2</sub>HPO<sub>4</sub>) was purchased from Innochem Technology Co., Ltd. (Beijing, China).

The parent H-ZSM-5 zeolite was treated by the following steps: First, the HZSM-5 zeolite powder was immersed in an aqueous solution of (NH<sub>4</sub>)<sub>2</sub>HPO<sub>4</sub> (0.15 mol/dm<sup>3</sup>), and the slurry was stirred for 2 h at 323 K and then dried by rotary evaporation at 313 K under reduced pressure. The obtained product was dried at 393 K overnight and calcined for 4 h at 873 K (heating rate, 0.167 K·s<sup>-1</sup>) in air. The amount of phosphorus was 1.2 wt% of the zeolite. The zeolites were pressed, crushed, screened, and 20–40 mesh zeolites were collected. Then, the zeolite was hydrothermally treated at 800 °C (heating rate, 0.111 K·s<sup>-1</sup>) for 4 h. Some studies reported similar methods to improve the stability of the zeolite [4,43].

#### 3.2. Catalyst Characterization

The crystallinity of the H-ZSM-5 zeolite was determined by X-ray diffraction (XRD) on an EMPYEEAN powder diffractometer (PANalytical Corporation, Alemlo, Netherland) with Cu Kα radiation (λ = 0.154 nm) at a scanning rate of 0.02° min<sup>-1</sup> from 5° to 35°. A nitrogen adsorption–desorption experiment was carried out at 77 K on a Micromeritics ASAP 2420 instrument to determine the specific surface areas and pore volume. The zeolite samples were activated under 10<sup>-2</sup> Pa for 4 h prior to the adsorption measurements. The Brunauer–Emmett–Teller (BET) equation was used to calculate the surface area and pore volume of zeolite. NH<sub>3</sub>-TPD experiments were carried out on an Autochem II 2920 (Micromeritics Instruments Corporation, Atlanta, GA, USA) unit equipped with a thermal conductivity detector. The zeolite sample (ca. 0.05 g) was pre-treated under a flow of helium at 400 °C for 1 h. After cooling to 150 °C, the sample was placed in a mixed gas flow of 10% NH<sub>3</sub> and 90% He (40 mL·min<sup>-1</sup>) and saturated with ammonia. After 60 min, the flow was switched to nitrogen, and the sample was heated from 150 to 600 °C at a rate of 10 °C·min<sup>-1</sup> under helium flow (40 mL·min<sup>-1</sup>). The desorbed ammonia was monitored by a thermal conductivity detector. The concentration of the Brønsted and Lewis acid sites was determined on a Bruker Vertex 80v FT-IR spectrometer (Salbruken, Germany). A self-supported catalyst wafer with a weight of 25 mg in an in situ cell with CaF<sub>2</sub> windows was heated to 400 °C for 1 h under 10<sup>-6</sup> Pa and then cooled to room temperature. A blank spectrum from 1300 to 1700 cm<sup>-1</sup> was recorded. Pyridine was adsorbed until equilibrium. Desorption was performed at 200 and 350 °C for 30 min, then the spectra of total acid and strong acid sites were recorded, respectively. The total acid concentration of fresh zeolite was 143.2 μmol·g<sup>-1</sup>; the surface area was 366 m<sup>2</sup>·g<sup>-1</sup>; the micropore volume was 0.171 cm<sup>3</sup>·g<sup>-1</sup>; the mesopore volume was 0.019 cm<sup>3</sup>·g<sup>-1</sup>. The total acid concentration of the regenerated zeolite (20 times) was 138.5 μmol·g<sup>-1</sup>; the surface area 352 m<sup>2</sup>·g<sup>-1</sup>; the micropore volume was 0.162 cm<sup>3</sup>·g<sup>-1</sup>; the mesopore volume was 0.023 cm<sup>3</sup>·g<sup>-1</sup>.

### 3.3. Reaction Equipment and Product Analysis

The pentene cracking experiments were performed in a continuous-flow fixed-bed reactor at atmospheric pressure. The feed was not diluted before entering the reactor. A diagram of the apparatus is shown in Figure 15.

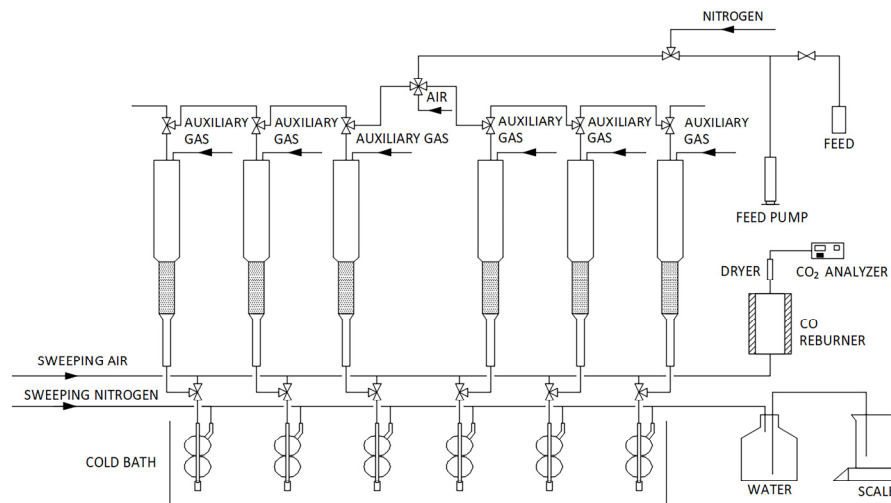


**Figure 15.** Fixed-bed reactor setup.

Six quartz tube reactors with a length of 420 mm (effective length of 150 mm) and an inner diameter of 6 mm were placed in the heating furnace. Thermocouples were placed at the center of the catalyst bed and 10 mm above the catalyst to ensure isothermal conditions. The 20–40 mesh catalyst was fixed using quartz wool at the bottom of the reactor.

Before the test, the whole system was swept with nitrogen. For each experimental run, the reactant feed was diluted with nitrogen, preheated to 150 °C, and injected into the reactor. After feeding, nitrogen was used to purge the catalyst bed in the reactor. The products were separated into the gas and liquid phases by a cool trap (−19 °C). The volumetric percentage of each component in the vapor was determined by an Agilent 6890 (Agilent Technologies Co., Ltd., Santa Clara, CA, USA) gas chromatograph (GC) equipped with a flame ionization detector (FID) and thermal conductivity detector (TCD). The mass of the vapor was calculated by the ideal gas equation. An Agilent 7890B (Agilent Technologies Co., Ltd., Santa Clara, CA, USA) gas chromatograph (GC) equipped with an OV-1 column (50 m × 0.2 mm × 0.5 μm) and a flame ionization detector was used to determine the mass percentage of each component for the liquid products. After the reaction, the temperature was raised to 670 °C (heating rate, 0.111 K·s<sup>−1</sup>), air (2 mL·s<sup>−1</sup>) was introduced for zeolite regeneration, and the resulting CO<sub>2</sub> was detected by a QGS-08B infrared carbon dioxide analyzer. The experiments with a mass balance of 95–105% were retained, and the others were discarded.

### 3.4. Operating Conditions and Reaction Indices

The pentene cracking experiments were performed under the following conditions: total pressure 130 kPa, partial pressure 60 kPa, reaction duration 70 s, time on the stream 0 s, temperature 500–750 °C, WHSV 15–83 h<sup>−1</sup>. Nitrogen was used as a dilution gas. The mass of the catalyst was 1 g.

The conversion of feed is defined as:

$$\text{Conversion}(C_5^=) = [m_i(C_5^=) - m_o(C_5^=)] / m_i(C_5^=) \times 100\% \quad (4)$$

where  $m_i(C_5^=)$  and  $m_o(C_5^=)$  are the mass flowrate of pentene in the inlet and outlet stream, respectively.

The molar selectivity of component  $C_i$  is defined as:

$$\text{Selectivity}(C_i) = n_o(C_i) / [n_i(C_5^-) - n_o(C_5^-)] \times 100\% \quad (5)$$

where  $n_o(C_i)$  is the molar flowrate of component  $C_i$  in the outlet stream,  $n_i(C_5^-)$  and  $n_o(C_5^-)$  are the molar flowrate of pentene at the inlet and outlet stream, respectively. Total aromatics is defined as the total of various  $C_6$ – $C_{10}$  aromatics.

The yield of component  $C_i$  is defined as:

$$\text{Yield}(C_i) = m_o(C_i) / m_i(C_5^-) \times 100\% \quad (6)$$

where  $m_o(C_i)$  is the mass flowrate of component  $C_i$  in the outlet stream, and  $m_i(C_5^-)$  is the mass flowrate of pentene in the inlet stream.  $C_5^+$  fraction is defined as  $C_6$ – $C_{10}$  hydrocarbon which does not include aromatics.

#### 4. Conclusions

The effects of reaction temperature and WHSV on the cracking of pentene to ethylene and propylene were investigated over H-ZSM-5. The ethylene selectivity increased with increasing temperature and decreased with increasing WHSV. The propylene selectivity reached a maximum with increasing temperature and WHSV. The total yield of ethylene and propylene reached a maximum (67.8 wt%) at 700 °C and 57 h<sup>-1</sup>.

Catalytic cracking contributed notably to the pentene cracking reaction over H-ZSM-5 at high temperatures. The proportion of pentene feed chemically adsorbed with the acid sites and cracked through catalytic cracking was above 88.4%, even at 750 °C. Ethylene and propylene in the products were mainly derived from catalytic cracking rather than thermal cracking at high temperatures. Based on the product distribution at various temperatures, the possible reaction network of pentene was summarized and estimated. The monomolecular cracking proportion increased from 1% at 500 °C to 95% at 750 °C. The increase in the monomolecular cracking proportion and the secondary cracking of butene were the main reasons for the high selectivity of ethylene and propylene at high temperatures. After 20 times of regeneration, the acidity and pore structure of the zeolite had little changed, and the conversion of pentene remained above 80% at 650 °C.

**Supplementary Materials:** The following supporting information can be downloaded at: <https://www.mdpi.com/article/10.3390/catal13010073/s1>, Table S1: Product yields from pentene cracking over quartz sand under various temperatures.

**Author Contributions:** Conceptualization, Y.H. and L.D.; methodology, Y.H.; validation, Y.Z., Y.X. and X.B.; formal analysis, Y.H.; investigation, L.D.; resources, Y.O. and Y.L.; data curation, Y.X.; writing—original draft preparation, Y.H. and Y.Z.; writing—review and editing, Y.H. and Y.X.; visualization, Y.H.; supervision, Y.X. and X.S.; project administration, Y.X.; funding acquisition, Y.X. All authors have read and agreed to the published version of the manuscript.

**Funding:** This research was funded by research grant from the National Key R&D program of China, grant number 2021YFA1501204 and Sinopec of China, grant number ST22001.

**Data Availability Statement:** Not applicable.

**Conflicts of Interest:** The authors declare no conflict of interest.

#### References

1. Gao, Y.; Neal, L.; Ding, D.; Wu, W.; Li, F. Recent Advances in Intensified Ethylene Production—A Review. *ACS Catal.* **2019**, *9*, 8592–8621. [[CrossRef](#)]
2. Propylene: 2022 World Market Outlook and Forecast Up to 2031. Available online: <https://mcgroup.co.uk/researches/propylene> (accessed on 3 May 2022).
3. Zhang, R.; Wang, Z. Catalytic cracking of 1-butene to propylene by Ag modified HZSM-5. *Chin. J. Chem. Eng.* **2015**, *23*, 1131–1137. [[CrossRef](#)]

4. Wattanapaphawong, P.; Reubroycharoen, P.; Mimura, N.; Sato, O.; Yamaguchi, A. Effect of carbon number on the production of propylene and ethylene by catalytic cracking of straight-chain alkanes over phosphorus-modified ZSM-5. *Fuel Process. Technol.* **2020**, *202*, 106367. [[CrossRef](#)]
5. Liu, W.; Placke, T.; Chau, K.T. Overview of batteries and battery management for electric vehicles. *Energy Rep.* **2022**, *8*, 4058–4084. [[CrossRef](#)]
6. Cong, X. The study on China's peak gasoline consumption from automobile industry changes. *Int. Pet. Econ.* **2019**, *27*, 60–70.
7. Fan, Y.; Bao, X.; Gang, S. H  $\beta$ /HZSM-5 Composite Carrier Supported Catalysts for Olefins Reduction of FCC Gasoline via Hydroisomerization and Aromatization. *Catal. Lett.* **2005**, *105*, 67–75. [[CrossRef](#)]
8. Sun, H.; Zhang, B.; Wei, C.; Cao, L.; Zhang, Y.; Zhao, L.; Gao, J.; Xu, C. Intensifying Ethylene and Propylene of Pentene Cracking of FCC Gasoline by Modulating the Brønsted Acid Site Concentrations. *Ind. Eng. Chem. Res.* **2021**, *60*, 17469–17479. [[CrossRef](#)]
9. Xu, Y.; Zuo, Y.; Bai, X.; Du, L.; Han, Y. Development background, development idea and conceptual design of FCC process for targeted cracking to light olefins. *Chin. Petrol. Process. Petrochem. Technol.* **2021**, *52*, 1–11.
10. Blay, V.; Epelde, E.; Miravalles, R.; Perea, L.A. Converting olefins to propene: Ethene to propene and olefin cracking. *Cat. Rev. Sci. Eng.* **2018**, *60*, 278–335. [[CrossRef](#)]
11. Chen, W.; Yi, X.; Liu, Z.; Tang, X.; Zheng, A. Carbocation chemistry confined in zeolites: Spectroscopic and theoretical characterizations. *Chem. Soc. Rev.* **2022**, *51*, 4337–4385. [[CrossRef](#)]
12. Lin, L.F.; Zhao, S.F.; Zhang, D.W.; Fan, H.; Liu, Y.M.; He, M.Y. Acid Strength Controlled Reaction Pathways for the Catalytic Cracking of 1-Pentene to Propene over ZSM-5. *ACS Catal.* **2015**, *5*, 4048–4059. [[CrossRef](#)]
13. Miyaji, A.; Sakamoto, Y.; Iwase, Y.; Yashima, T.; Koide, R.; Motokura, K.; Baba, T. Selective production of ethylene and propylene via monomolecular cracking of pentene over proton-exchanged zeolites: Pentene cracking mechanism determined by spatial volume of zeolite cavity. *J. Catal.* **2013**, *302*, 101–114. [[CrossRef](#)]
14. Zhu, X.; Liu, S.; Song, Y.; Xie, S.; Xu, L. Catalytic cracking of 1-butene to propene and ethene on MCM-22 zeolite. *Appl. Catal. A Gen.* **2005**, *290*, 191–199. [[CrossRef](#)]
15. Chen, J.; Yan, H.; Gong, H.; Zhang, H.; Zhou, Y.; Gao, C.; Liu, Y.; Chen, X.; Yang, C. Tetrahedrally coordinated W (VI) species induced Lewis acid for stable catalytic cracking of 1-hexene to propene. *Chem. Eng. J.* **2022**, *448*, 137504. [[CrossRef](#)]
16. Sun, H.; Cao, L.; Zhang, Y.; Zhao, L.; Gao, J.; Xu, C. Effect of Catalyst Acidity and Reaction Temperature on Hexene Cracking Reaction to Produce Propylene. *Energy Fuel* **2021**, *35*, 3295–3306. [[CrossRef](#)]
17. Berta, A.H.; Hwang, H.D.; Asfha, H.B.; Kang, N.Y.; Kim, K.; Park, Y.-K. Reaction mechanism and kinetic modeling of olefin conversion over phosphorus modified ZSM-5 catalyst. *Korean J. Chem. Eng.* **2022**, *39*, 1460–1471. [[CrossRef](#)]
18. Huang, X.; Aihemaitijiang, D.; Xiao, W.-D. Reaction pathway and kinetics of C3–C7 olefin transformation over high-silicon HZSM-5 zeolite at 400–490 °C. *Chem. Eng. J.* **2015**, *280*, 222–232. [[CrossRef](#)]
19. Aretin, T.V.; Schallmoser, S.; Standl, S.; Tonigold, M.; Lercher, J.A.; Hinrichsen, O. Single-event kinetic model for 1-pentene cracking on ZSM-5. *Ind. Eng. Chem. Res.* **2015**, *54*, 11792–11803. [[CrossRef](#)]
20. Aretin, T.V.; Hinrichsen, O. Single-Event Kinetic Model for Cracking and Isomerization of 1-Hexene on ZSM-5. *Ind. Eng. Chem. Res.* **2014**, *53*, 19460–19470. [[CrossRef](#)]
21. Chen, C.-J.; Rangarajan, S.; Hill, I.M.; Bhan, A. Kinetics and Thermochemistry of C4–C6 Olefin Cracking on H-ZSM-5. *ACS Catal.* **2014**, *4*, 2319–2327. [[CrossRef](#)]
22. Zhang, R.; Wang, Z.; Liu, H.; Liu, Z.; Liu, G.; Meng, X. Thermodynamic equilibrium distribution of light olefins in catalytic pyrolysis. *Appl. Catal. A Gen.* **2016**, *522*, 165–171. [[CrossRef](#)]
23. Warnecke, F.; Lin, L.; Haag, S.; Freund, H. Identification of Reaction Pathways and Kinetic Modeling of Olefin Interconversion over an H-ZSM-5 Catalyst. *Ind. Eng. Chem. Res.* **2020**, *59*, 12696–12709. [[CrossRef](#)]
24. Standl, S.; Kühlewind, T.; Tonigold, M.; Hinrichsen, O. On Reaction Pathways and Intermediates during Catalytic Olefin Cracking over ZSM-5. *Ind. Eng. Chem. Res.* **2019**, *58*, 18107–18124. [[CrossRef](#)]
25. Li, J.; Li, T.; Ma, H.; Sun, Q.; Li, C.; Ying, W.; Fang, D. Kinetics of coupling cracking of butene and pentene on modified HZSM-5 catalyst. *Chem. Eng. J.* **2018**, *346*, 397–405. [[CrossRef](#)]
26. Sadrameli, S.M. Thermal/catalytic cracking of hydrocarbons for the production of olefins: A state-of-the-art review I: Thermal cracking review. *Fuel* **2015**, *140*, 102–115. [[CrossRef](#)]
27. Poutsma, M.L. Fundamental reactions of free radicals relevant to pyrolysis reactions. *J. Anal. Appl. Pyrolysis* **2000**, *54*, 5–35. [[CrossRef](#)]
28. Sadrameli, S.M. Thermal/catalytic cracking of liquid hydrocarbons for the production of olefins: A state-of-the-art review II: Catalytic cracking review. *Fuel* **2016**, *173*, 285–297. [[CrossRef](#)]
29. Fakhroleslam, M.; Sadrameli, S.M. Thermal/catalytic cracking of hydrocarbons for the production of olefins; a state-of-the-art review III: Process modeling and simulation. *Fuel* **2019**, *252*, 553–566. [[CrossRef](#)]
30. Buchanan, J.S.; Santiesteban, J.G.; Haag, W.O. Mechanistic Considerations in Acid-Catalyzed Cracking of Olefins. *J. Catal.* **1996**, *158*, 279–287. [[CrossRef](#)]
31. Yamaguchi, A.; Jin, D.; Ikeda, T.; Sato, K.; Hiyoshi, N.; Hanaoka, T.; Mizukami, F.; Shirai, M. P-ZSM-5 Pretreated by High-Temperature Calcination as Durable Catalysts for Steam Cracking of n-Hexane. *Catal. Lett.* **2014**, *144*, 44–49. [[CrossRef](#)]

32. Kubo, K.; Iida, H.; Namba, S.; Igarashi, A. Comparison of steaming stability of Cu-ZSM-5 with those of Ag-ZSM-5, P/H-ZSM-5, and H-ZSM-5 zeolites as naphtha cracking catalysts to produce light olefin at high temperatures. *Appl. Catal. A Gen.* **2015**, *489*, 272–279. [[CrossRef](#)]
33. Lin, L.; Qiu, C.; Zhuo, Z.; Zhang, D.; Zhao, S.; Wu, H.; Liu, Y.; He, M. Acid strength controlled reaction pathways for the catalytic cracking of 1-butene to propene over ZSM-5. *J. Catal.* **2014**, *309*, 136–145. [[CrossRef](#)]
34. Choudhary, V.R.; Banerjee, S.; Panjala, D. Influence of Temperature on the Product Selectivity and Distribution of Aromatics and C8 Aromatic Isomers in the Conversion of Dilute Ethene over H-GaAlMFI (ZSM-5 type) Zeolite. *J. Catal.* **2002**, *205*, 398–403. [[CrossRef](#)]
35. Chen, Z.; Song, W.; Hou, Y.; Wang, H.; Qian, W. Temperature-dependent secondary conversion of primary products from methanol aromatization in a two-stage fluidized bed. *Fuel* **2020**, *267*, 117204. [[CrossRef](#)]
36. Choudhary, V.R.; Banerjee, S.; Panjala, D. Product distribution in the aromatization of dilute ethene over H-GaAlMFI zeolite: Effect of space velocity. *Microporous Mesoporous Mater.* **2002**, *51*, 203–210. [[CrossRef](#)]
37. Sazama, P.; Dědeek, J.; Gábová, V.; Wichterlová, B.; Spoto, G.; Bordiga, S. Effect of aluminium distribution in the framework of ZSM-5 on hydrocarbon transformation. Cracking of 1-butene. *J. Catal.* **2008**, *254*, 180–189. [[CrossRef](#)]
38. Hou, X.; Ni, N.; Wang, Y.; Zhu, W.; Qiu, Y.; Diao, Z.; Liu, G.; Zhang, X. Roles of the free radical and carbenium ion mechanisms in pentane cracking to produce light olefins. *J. Anal. Appl. Pyrolysis* **2019**, *138*, 270–280. [[CrossRef](#)]
39. Longstaff, D.C. Naphtha cracking kinetics and process chemistry on Y and ZSM5 type catalysts. *Energy Fuel* **2019**, *33*, 2445–2452. [[CrossRef](#)]
40. Teraishi, K. Computational study on the product selectivity of FCC zeolitic catalyst. *J. Mol. Catal. A Chem.* **1998**, *132*, 73–85. [[CrossRef](#)]
41. Ma, Z.; Hou, X.; Chen, B.; Zhao, L.; Yuan, E.; Cui, T. Analysis of n-hexane, 1-hexene, cyclohexane and cyclohexene catalytic cracking over HZSM-5 zeolites: Effects of molecular structure. *React. Chem. Eng.* **2022**, *7*, 1762–1778. [[CrossRef](#)]
42. Castro-Marcano, F.; van Duin, A.C.T. Comparison of thermal and catalytic cracking of 1-heptene from ReaxFF reactive molecular dynamics simulations. *Combust. Flame* **2013**, *160*, 766–775. [[CrossRef](#)]
43. Lukyanov, D.B. Reactivity of Propene, n-Butene, and Isobutene in the Hydrogen Transfer Steps of n-Hexane Cracking over Zeolites of Different Structure. *J. Catal.* **1994**, *147*, 494–499. [[CrossRef](#)]

**Disclaimer/Publisher’s Note:** The statements, opinions and data contained in all publications are solely those of the individual author(s) and contributor(s) and not of MDPI and/or the editor(s). MDPI and/or the editor(s) disclaim responsibility for any injury to people or property resulting from any ideas, methods, instructions or products referred to in the content.